EXPERIMENTAL, THEORETICAL, AND NUMERICAL MODAL ANALYSIS OF A DAMPED PORTABLE-GRINDER DISK

Angelo Farina, Rinaldo Garziera, and Sara Rainieri
Università di Parma, Dip. Ing. Ind.
V.le delle Scienze, 43100 Parma

ABSTRACT

This paper deals with a theoretical and experimental investigation into the vibration of portable grinder disks. Our research objective is to determine the elasto-dynamic properties for a new type of *damped* disk and evaluate their behavior in terms of reduction in noise emission levels.

The disk vibration has been studied from a variety of standpoints. A comparison between the vibration modes obtained from theory and experimental data allows us to estimate the constitutive parameters of these new disks. In addition, our study includes a numerical analysis that takes into account the effects of the disk rotation. Theoretical modes show good agreement with experimental data. They both confirm a reduction in the high frequency modes exhibited by the *damped* disk when compared to the *undamped* disk. The finite element analysis allows prediction for the shift in natural frequencies produced by the centrifugal force field acting on the disk surface.

NOMENCLATURE

SPL	sound pressure level
η	band–average loss factor
E	Young's module
h	disk thickness
κ	Poisson's ratio
w	z direction displacement
μ	mass dens. per unit area
ω	frequency of vibration
r_i	inner radius
r_e	outer radius
m, n	modes numbers
σ_r, σ_t	radial and tangential stress
J, I, Y, K,	Bessel functions
V	energy

1 INTRODUCTION

Portable grinders are widely used tools, suitable in a wide variety of metal manufacturing processes such as cutting or finishing surfaces etc. Grinders emit high levels of noise: emission can reach levels above 110 dB(A).

Increasing interest in acoustic pollution control has encouraged development into new methods for reducing acoustic emission of industrial machinery. Since acoustic emission is generally connected with the vibration of some machine components, much of today's research is devoted to vibration control. Most of the grinder's noise is emitted through the vibration of its disk. Passive control by means of appropriate internal damping of these vibrations seems, therefore, to be the most efficient method in reducing noise and alleviating discomfort for the machine operator.

One of the techniques adopted in order to damp vibration is to build layered disks. This technology has also been applied, with effective results, in other fields [1]. Layered grinder disks are made by casting a sort of rubber layer in the common abrasive agglomerate, which performs a high internal damping action through its hysteresis.

The experimental noise emission tests and modal analysis here presented have been carried out for two classes of grinder disks: the *non damped* disks, referred to as "normal", and the *damped* disks, referred to as "Silentium".

This article focuses on the elastic parameters and loss factor estimation for these new "Silentium" disks. The Poisson's ratio κ and Young Module E are important for the characterization of the tested material and for the prediction of the natural frequencies. Knowledge of these two parameters constitutes the basis for eventual numerical investigation. These parameters have been calculated in section 7, via a comparison between experimental and calculated frequencies. The loss factor has been worked out from a series of acoustic measurements as described in section 3 for both classes of disks. This allows for a comparison between the performances of the two disks in terms of noise emission reduction. The comparison between "normal" and "Silentium" disks is a constant theme throughout the present paper which basically includes four parts: experiments on the disks from which natural frequencies, mode shapes and

loss factor have been calculated; the solution of free vibrations for a disk clamped on the inner circumference and free at the external boundary; estimation of parameters through the comparing of experimental and theoretical frequencies; a finite element modal analysis that takes into account the disk rotation and graphically shows the first modes.
Furthermore, the direct evaluation of the loss factor allows for the estimation of the damping properties of the material inserted in the new disk versus frequency.

2 MODAL EXPERIMENTAL TESTS

The experiments deal with two kinds of grinder disks, namely the "normal" and the "Silentium". From each of these two types ten different disks were taken with diameters ranging from 230 mm to 115 mm and a thickness of 7 mm. Most of the tests were performed on a $r_e = 178$ mm disk. In order to reproduce clamping conditions as similar as possible to actual working conditions, the disk was fixed to a grinder shaft clamped in a solid vice fixed on a specific table. The experimental apparatus is shown in figure 1.

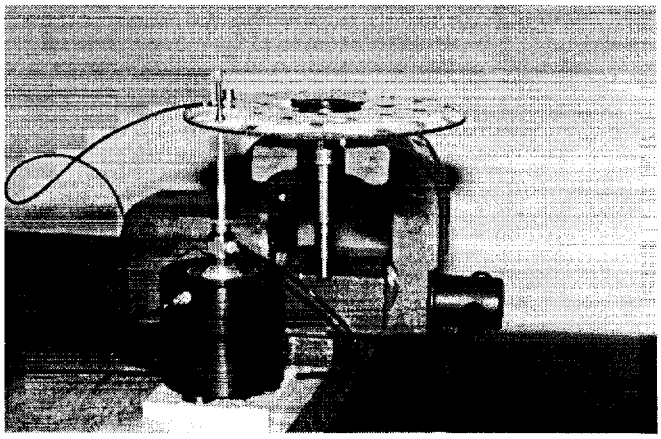

Figure 1: *The disk mounted on a vice.*

Two different excitation techniques were used to test the disk. Hammer excitation was chosen to measure the *decay time*, while an electrodynamic shaker was employed to accurately measure the *modal frequencies* and the *modal shapes*. The applied forces were sampled through a Brüel & Kjær (B&K) load cell, by mounting either the hammer (B&K type 8203) or the shaker (B&K type 4810). Accelerations were read using a B&K accelerometer (type 4393) with a mass of 2.4 g.
In order to simulate the force exchanged between the disk and the surface being ground, the excitation point was chosen on the external circumference. During grinding, the tangential forces excite only *mute modes*. Therefore, the applied force direction was kept perpendicular to the disk surface. The test points were disposed on a grid dividing the disk surface in 7 rows and 7 columns. The grid points off the disk were not measured. The data were acquired through two B&K type 2635 charge amplifiers, connected to both a two channel FFT spectrum analyzer (OnoSokki CF920), and a PC A/D board (A2D160, DRA laborat.). Noise excitation was produced by a PC-A/D board, incorporating an MLS (Maximum Length Sequence) pseudo-random noise generator [2].
The deterministic nature of the test signal proved advantageous in facilitating the analysis of the collected data, performed on a PC. It allowed for quick computation of the impulse response through a *fast Hadamard transform* [3], which directly provides the time domain response through simple additions and subtractions. On the other hand, the FFT analyzer was working in the traditional way, computing the Frequency Response Function (FRF) via the FFT spectra.
As shown in figure 2, the damping of the material is quite high, thus making the impulse response fade away rapidly (about 50 ms). Hence we can acquire up to 4096 points at a sampling rate of 30 kHz, which corresponds to a time length of approximately 130 ms.

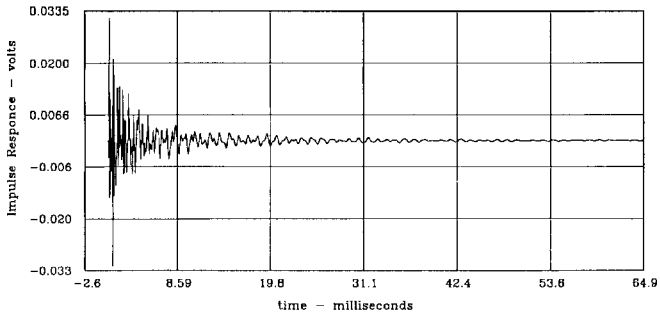

Figure 2: *Impulse response for damped disks (MLS deconvolution).*

Comparing the effectiveness of the two acquisition instruments, it can be said that the "MLS A/D" PC-board gives significant benefits when compared with the standard FFT analyzer in terms of acquisition speed (no averaging is required), frequency resolution, and signal to noise ratio improvement.

3 ACOUSTIC DATA MEASUREMENT

The noise emitted from the grinding disks during their normal operation was measured according to the ISO test codes 3744 and 11201 and to AFNOR E 65–131 which specify the microphones' position. A certain amount of radiated noise may come from the piece being ground. Since standards do not treat this case in a rigorous way, we reduced the sound radiated by the metal rod as much as possible. A special support was formed by a solid wood block bearing a mild steel mass. On this steel block, a robust gripping mechanism constituted by two jaws held the rod of mild steel being

ground. The steel mass has a workable surface 20 mm wide and 300 mm long. The system was heavily damped by the insertion of damping rubber sheets between all the metal-to-metal joints. The tests were conducted outdoors, in a quiet place, far from buildings and roads.

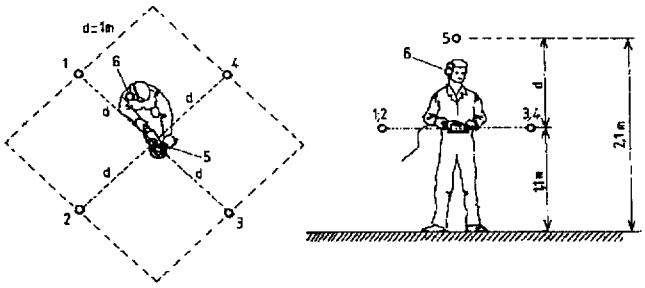

Figure 3: *Microphones layout.*

In figure 3 the six microphones layout is shown. Five microphones were placed at one meter from the average position of the grinding tool and in direct sight of the sound source. The sixth microphone was placed near the operator's right ear, attached to the protective plastic screen worn by the operator. The angle between the disk and the rod surface being ground was maintained at 25^o. All six microphones were Brüel & Kjær (B&K) type 4165, coupled with (B&K) type 2645 preamplifiers and (B&K) type 2804 power supplies.

The first four microphone outputs were recorded by a TEAC RD 101-T DAT recorder, while microphone five and six were connected to a CASIO DA-7 DAT recorder. The noise emitted from the tool was found to be negligible when compared with the noise emitted from the disks. The digital recordings have been analyzed in the laboratory through both a (B&K) type 2133 real time analyzer and an OnoSokki CF-920 FFT analyzer (put in 800 lines mode).

Measurements were done on ten different disk types: five different diameters, ranging from 230 mm to 115 mm, by two kinds of grinding disks, namely "normal" and "Silentium". The results were linearly averaged over a one minute recording time. In order to test whether the measurements were reproducible, three different samples were collected from every disk, each with a different human operator. An electric grinding tool *Metabo* running at 8500 r.p.m. was used.

Results from the experiments using 178 mm disks are of great interest. In this case the *Sound Pressure Levels* (SPL) are quite high for the "normal" disk while the "Silentium" disk exhibits a significant reduction in the overall A-weighted SPL.

In table 1 the A-Weighted SPL values (at the operator ear and averaged over the other five microphones) for the five disk diameters are reported.

The spectral analysis also shows noticeable differences between the two grinding materials, as can be seen in figure 4, in which the averaged 800-lines spectra for the two 178 mm disks are reported.

	SPL (dBA)		SPL (dBA)	
Disk diam.	"N"	"S"	"N"	"S"
230 mm	114.3	109.6	102.5	97.4
178 mm	114.8	108.4	103.1	93.6
150 mm	111.8	106.7	99.1	92.7
125 mm	110.3	109.3	97.6	94.2
115 mm	109.9	109.7	99.5	97.0

Table 1: *Sound Pressure Levels (dBA) for* non damped *and* damped *disks.*

The effect of the damping material becomes evident at frequencies above 1000 Hz, where the strong peaks of the "normal" disk disappear completely. At lower frequencies the peaks are still present, but their amplitude is reduced by approximately 6 dB. In this case there was an overall reduction in the A–weighted SPL of about 8 dB(A).

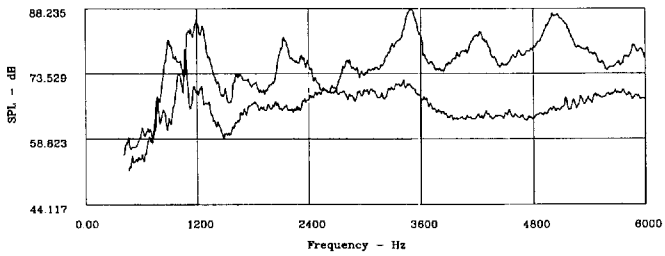

Figure 4: *SPL narrow-band spectra of "normal" and "Silentium" disks.*

From the analysis of the acoustical data, two effects of disk rotation are observed. Firstly, the frequencies increase by about 3% for the first mode; this is explained in section 8. Secondly, the rotation frequency combines with the vibration frequencies, so that acoustic radiation arises at frequencies shifted of $\pm n\omega_r$ from that of the non rotating disk, ω_r being the rotation speed and n being the mode number. We can estimate this speed about 6200 R.P.M. for an actually grinding tool. With reference to the mentioned effects, figure 5 (starting from the bottom) shows the FRF for an undamped disk, the frequencies shift and the mode splitting due to rotation in the acoustic measured spectrum. These two effects are further discussed in sections 6 and 8.

4 EVALUATING MODES fROM EXPERIMENTS

To find modal frequencies and shapes, all of the FRF's were added together following an energy criteria, thus sharpening the resonances. Analysis of this FRF sum was performed

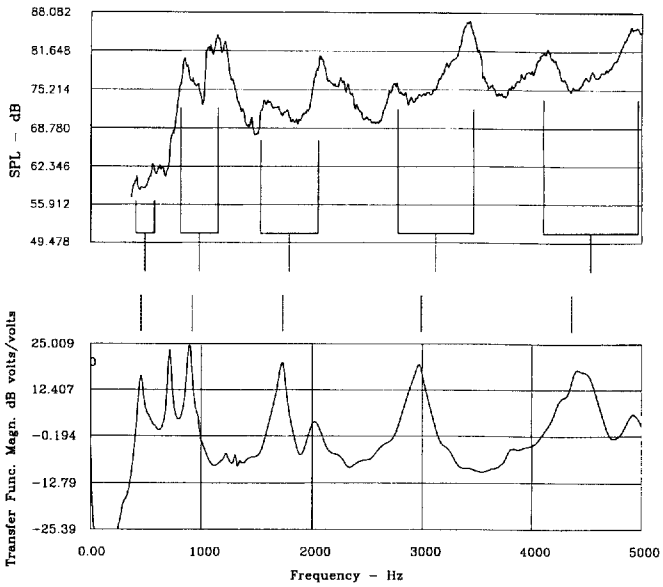

Figure 5: *From the bottom: FRF for an undamped disk, frequencies shift and mode splitting due to rotation in the acoustic measured spectrum.*

via a three point circle fitting code which takes into account only three spectral lines: the main line and the adjacent ones. This code, developed by one of the authors of this paper, is now part of a general purpose code called *OnoRead*, copyrighted by ONO–SOKKI co. Ltd. The modes are well separated, therefore it is possible to manually identify and analyze the spectrum peaks, as can be seen in figure 6.

For a given frequency range, centered on a peak, the computer code extracts the modal amplitude and phase. The code can also produce a graphic animation of the disk while vibrating. The modal shapes are essentially the same for the damped and the undamped disks, while the maximum displacement and the modal frequencies are lower for the damped disks. Table 3 reports the first six frequencies for modes without circumference nodes.

n	Natural freq. (Hz)	Degenerated freq. (Hz)
0	735	735
1	475	333
		617
2	910	627
		1193
3	1730	1305
		2015
4	2950	2383
		3517

Table 2: *Natural and degenerated frequencies (Hz) for* non damped *disks.*

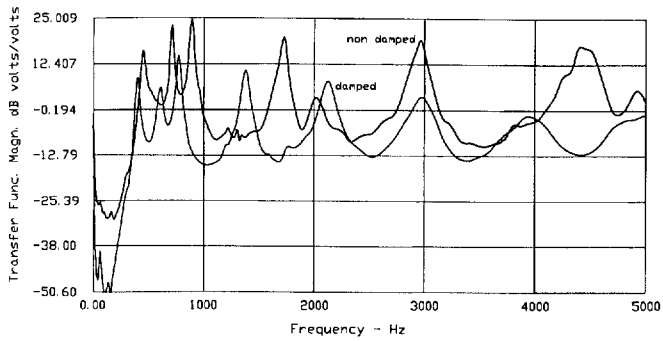

Figure 6: *FRF curves for undamped and "Silentium" disks (all test points averaged).*

n	0	1	2	3	4	5
normal	735	505	915	1730	2950	4452
Silentium	635	440	815	1420	2395	3610

Table 3: *Frequencies (Hz) of modes* $(0, n)$ *for* non damped *(normal) and* damped *(Silentium) disks.*

5 DAMPING MEASUREMENT

Damping measurement requires hammer excitation, in order to avoid the shaker damping affecting the decay time of the vibrating system. In addition, the decay time is frequency-dependent. At natural frequencies the decay time is usually longer than at frequencies out of resonance. While the standard approach is to measure the decay time only at the natural frequencies, in this study we follow a different approach: the impulse response is digitally filtered with band-pass filters of 1/3 octave, and each filtered response is then backwardly integrated, as suggested in [4]. As a result, the decay of an interrupted stationary band–pass noise signal is reconstructed, as shown in figure 7.

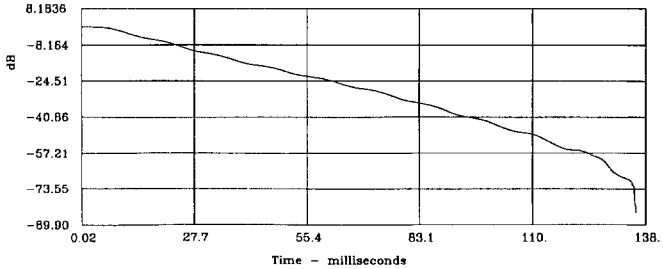

Figure 7: *Backward integrated decay curve. (Filtered Schroeder Plot 100 kHz, 0.33 oct).*

The slope of the decay curve gives the reverberation time "RT60" (time required for a 60 dB decay). Finally the band-average loss factor can be computed as

$$\eta = \frac{1}{2\pi}\left[1 - 10^{\left(\frac{-6}{RT60 f_c}\right)}\right] \quad . \tag{1}$$

The loss factor measurement was repeated for each frequency band upon all the measurement points, and then an average value was computed at each frequency f_c for both the "normal" and "Silentium" disks. Figure 8 shows the comparison between these loss factor measurements.

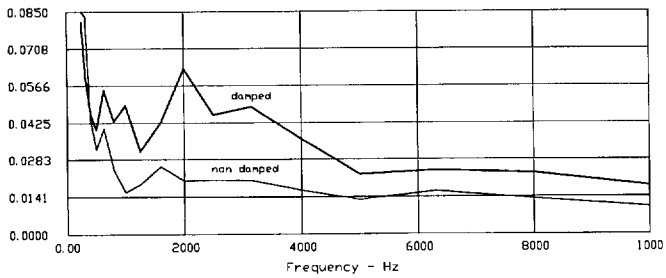

Figure 8: *Loss factors of "normal" and "Silentium" disks.*

A substantial increase in damping obtained through the new type of grinding disks is evident. It can be stated that, on frequency average, the damped disk shows a loss factor 2.5 times greater than that of the undamped disk, while in the noisiest range (2 - 4 kHz) the ratio between the two loss factors reaches 3.
In terms of resonance peaks magnification, this suggests an expected peak amplitude reduction of $20\log(3) = 9.54$ dB. This peak amplitude reduction was effectively achieved in an acoustically measured spectra.

6 THEORETICAL MODES EVALUATION

This section presents the solution for the free vibrations of a spinning circular plate clamped on its inner circumference r_i and free at r_e. Although this theory is known in literature, see for example [5], we shortly report it in order to define some quantities used in the paper.
We assume that the plate is lying in the xy plane with the deflection $w(x, y, t)$ taking place along the z direction. We also assume that the deflection is small compared to the plate dimensions, that no tangential action is present on the surface of the disk and in addition to this we do not take into consideration the rotatory inertia forces due to bending. The displacement equation of motion for the free vibration is (see for example [6])

$$\frac{Eh^3}{12(1-\kappa^2)}\nabla^2(\nabla^2 w) + \mu\frac{\partial^2 w}{\partial t^2} = 0 \tag{2}$$

where E denotes Young's modulus, μ is the mass density per unit surface area and κ is the Poisson's ratio. Assuming a set of time dependent cylindrical coordinates and stating

$$\Gamma(\vartheta, \tau) = \cos\left[n(\vartheta - \omega_r\tau) + \varphi\right] cos(\omega\tau + \psi) \ , \tag{3}$$

where ω is the generic natural frequency, the general solution for the free vibrations may be expressed as the product of two sets of functions

$$w = [a_n J_n(\gamma r) + b_n I_n(\gamma r) + c_n Y_n(\gamma r) + d_n K_n(\gamma r)] \cos\left[n(\vartheta - \omega_r\tau) + \varphi\right]\cos(\omega\tau + \psi) \ , \tag{4}$$

where we have defined

$$\gamma = \frac{12(1-\kappa^2)\mu\omega^2}{Eh^3} \ .$$

The first term of the product gives the radial shape of the disk, and contains Bessel functions and Modified Bessel functions of the first and second kind. The second term shows how the diametrical nodes depend on n and how the disk rotation affects the natural vibration frequencies of the plate. By ignoring the centrifugal forces acting on the plate, the only effect of the spinning is to produce a modulation in the vibration; in fact writing

$$\Gamma(\vartheta, \tau) = \frac{1}{2}\cos\left[n\vartheta + (\omega - n\omega_r)\tau + \alpha\right] + \frac{1}{2}\cos\left[n\vartheta + (\omega + n\omega_r)\tau + \beta\right] \tag{5}$$

the vibration frequency results shifted by $\pm n\omega_r$, where n refers to the diametrical nodes.
A first boundary condition states the congruence of displacements along circumferences

$$w(r, \vartheta, \tau) = w(r, \vartheta + 2\pi, \tau) \tag{6}$$

from this equation and equation 4 it follows that n must be an integer, that is: only Bessel functions of integer order have to be considered. For the clamped circumference the deflection and the slope of deflection must be zero

$$\begin{cases} w(r, \vartheta) = 0 & \text{for } r = r_i \\ \dfrac{\partial w}{\partial r} = 0 & \text{for } r = r_i \ . \end{cases} \tag{7}$$

For the free edge the bending moment and the shearing force must be zero ($r = r_e$).

$$\begin{cases} \dfrac{1}{\kappa}\dfrac{\partial^2 w}{\partial r^2} + \dfrac{1}{r}\dfrac{\partial w}{\partial r} + \dfrac{1}{r^2}\dfrac{\partial^2 w}{\partial \vartheta^2} = 0 \\ \dfrac{\partial}{\partial r}\left(\dfrac{\partial^2 w}{\partial r^2} + \dfrac{1}{r}\dfrac{\partial w}{\partial r} + \dfrac{1}{r^2}\dfrac{\partial^2 w}{\partial \vartheta^2}\right) + \dfrac{1-\kappa}{r^2}\dfrac{\partial^2}{\partial \vartheta^2}\left(\dfrac{\partial w}{\partial r} - \dfrac{w}{r}\right) = 0 \ . \end{cases} \tag{8}$$

Applying these conditions to equation 4 we find at each n an homogeneous system of four equations with $v = \{a_n\,, b_n\,, c_n\,, d_n\}^t$ unknown,

$$Z_n v_n = 0\,. \tag{9}$$

The coefficients of these four equations may be set in a 4×4 matrix, say Z_n, whose determinant must be equal to zero in order to obtain a non trivial solution for v. The elements of Z_n matrix are reported in full details in appendix A.
The determinant of matrix Z_n depends on r_i , r_e , γ and κ, while it does not depend on E. At any integer number n, which gives the number of diametrical nodes, we find infinite values of γ, say $\gamma_{n,m}$, satisfying equation $det(Z_n) = 0$, m giving the number of circumference nodes. Finally we can find the natural frequencies ω from the definition of γ. It can also be noted that $det(Z_n)$ depends only on the two products γr_i γr_e and on the two parameters n and κ, (see appendix A), so we may find, for example, solutions of $\det(Z_n)$ in term of $\gamma_{n,m} r_e$ given the ratio r_i/r_e , the Poisson's ratio κ, and n. Zeros of $det(Z_n)$ can be found with a simple bisecting routine since $det(Z_n)$ is a smooth and well behaved function.

7 EXPERIMENTAL AND THEORETICAL DATA COMPARISON VERSUS PARAMETERS ESTIMATION

This section suggests a possible way to determine system parameter Poisson's ratio κ and Young's module E. We point out that all the considerations and comparisons here made are intended for a disk at rest (not spinning). We recall equation 9. Since the value of $\det(Z_n)$ depends on Poisson's ratio κ, which is unknown, a straightforward solution for the eigenvalues is not possible. In this section we make deep use for the quantity $\det(Z_n)$, which was derived in the previous section for a spinning disk. We remark, however, that $\det(Z_n)$ does not depend on the spinning, so it can be used for the next considerations.
For a non spinning disk, apart from the true clamping radius, the boundary fixing and clamping conditions do not affect the results (as would have been the case for a rotating disk, see example [7]).
While the value of ω varies with the square root of E, the ratio between two frequencies, say for example $\nu = \omega^2_{3,2}/\omega^2_{5,4}$, does not depend on Young's module. Therefore, we can calculate κ by matching the ratio between any two experimental frequencies with the ratio between the two corresponding calculated frequencies.
We can for example consider the ratio

$$\nu = \frac{\gamma_{0,0}}{\gamma_{5,0}} = \nu(\kappa)\,, \tag{10}$$

between two well experimental evaluated frequencies, obtaining an approximate estimation of ν and of the rate $\mathrm{d}\nu/\mathrm{d}\kappa$ thus we are able to calculate a better value of ν using the Newton-Rapson formula

$$\kappa_{i+1} = \kappa_i - \nu(\kappa_i)\frac{\mathrm{d}\kappa}{\mathrm{d}\nu}\Big|_{\kappa_i}\,. \tag{11}$$

This method is sufficiently precise after only a few iterations. Table 4 shows the characteristics of the two disks, "normal" and "Silentium". The results in table 4 were obtained by applying the above mentioned methods to the experimental data reported in section 2.

Undamped	Silentium
$\omega_{0,0} = 4618$ rad/s	$\omega_{0,0} = 3990$ rad/s
$\omega_{3,0} = 10870$ rad/s	$\omega_{3,0} = 8922$ rad/s
$\rho = 2560$ kg/m^3	$\rho = 2560$ kg/m^3
$\kappa = 0.19$	$\kappa = 0.26$
$E = 1.88e10$ N/m^2	$E = 1.31e10$ N/m^2

Table 4: *Properties of standard and Silentium disks.*

The interpretation of these values must take into account the fact that the nature of the disk material is not homogeneous. The *damped* disk is made of an abrasive agglomerate plus a rubber net lying in a *sandwich-like* manner in the middle of the disk.
This kind of structure may recall layered materials for which specific and relatively complex theories have been developed [8]. In spite of this, at present, it seems appropriate and sufficient to consider a homogeneous continuous. The elastic properties reported in table 4 should be considered as belonging to this model.
Table 5 reports the experimental and the calculated frequencies for both, *undamped* and "Silentium" disks. The calculated values have been analytically obtained using the elastic properties of table 4. The comparison contained in table 5 shows a very good agreement between experimental and theoretical data.

8 Numerical solution with centrifugal force

In order to find modes and frequencies of the disk in operating condition, i.e. while spinning at 890 rad/s, centrifugal forces must be taken into account. In presence of a radial tension σ_r and a tangential tension σ_t, equation 2 becomes

$$\frac{Eh^3}{12(1-\kappa^2)}\nabla^2(\nabla^2 w) + \mu\frac{\partial^2 w}{\partial t^2} - \frac{h}{r}\frac{\partial}{\partial r}\left(\sigma_r\, r\frac{\partial w}{\partial r}\right) - \frac{h}{r^2}\,\sigma_t\,\frac{\partial^2 w}{\partial \vartheta^2} = 0 \tag{12}$$

which can be integrated numerically, for example, by using finite element analysis. The model for the finite element

	undamped disk			Sil. disk		
m,n	exp.	calc.	diff.	exp.	calc.	diff.
0,0	735	736	0 %	635	635	0 %
0,1	505	721	30 %	440	615	28 %
0,2	915	953	4 %	815	787	- 3 %
0,3	1730	1728	0 %	1420	1422	0 %
0,4	2950	2929	0 %	2395	2419	1 %
0,5	4452	4458	0 %	3610	3693	2 %
1,0	–	4718	–	–	4039	–
1,1	–	5003	–	–	4273	–
1,2	–	5903	–	–	5019	–
1,3	–	7490	–	–	6347	–
1,4	–	9748	–	–	8247	–
1,5	–	12575	–	–	10631	–
2,0	–	13790	–	–	11756	–

Table 5: *Comparison between experimental and calculated frequencies (Hz) of* undamped *and Silentium disks (at rest).*

analysis, consists of 448 "plate elements" in which all the degrees of freedom are frozen for the nodes belonging to the inner circumference of radius r_i. To better investigate the frequency shift due to the inertia forces acting on the disk, several runs corresponding to different values of the rotation frequency were carried out.
The centrifugal forces acting on each element were calculated considering the different values of rotation frequency ω_r and these were applied to the inner nodes of the elements themselves. These inertia forces in the case of $\omega_r = 890\,\text{rad/s}$ vary from about 20 N on the inner elements to 70 N on the outer ones. From this finite element model we obtain the common flexural modes together with the so called "membrane modes" which do not involve any disk bending. These non bending modes do not produce any sound, therefore, they are of little importance and thus not reported.

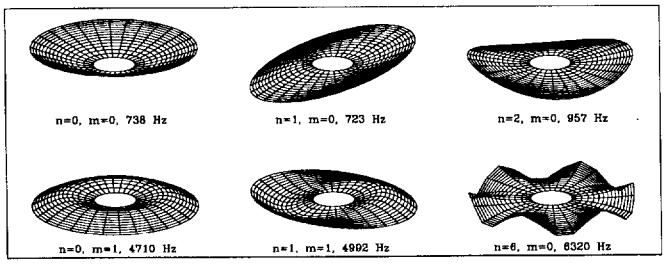

Figure 9: *Disk modes obtained from finite element analysis.*

The frequencies of the first five modes, obtained from the finite element analysis of the non damped disk with $\omega_r = 142\,\text{Hz}$, result about 3% higher compared with those reported in tables 5. This shift is only due to the centrifugal forces, since a finite element analysis of the same model without these inertia forces results in frequencies that are very similar to the values of tables 5. For higher values of ω_r, the shift in frequency due to the centrifugal forces is significant. Table 6 shows the frequency shift of the first mode, together with the values of the rotation frequency considered.

ω_r(rad/s)	$\Delta\omega_{1,0}$(Hz)
890	18.8
1335	41.7
1780	72.7
2225	110.7
2670	154.9

Table 6: *Frequency shift of the first mode*

The eigen–function corresponding to this mode can be obtained from equation 9, taking $n = 1$. Substituting the values of $\omega_{1,0}, \kappa, E$ calculated in section 7 and taking $a_1 = 1$, for instance, the vector v is given by

$$v = \{1.0, 0.3, 1.4, 1.1\}\,. \tag{13}$$

The radial and tangential tension due to the inertial forces acting on the disk depends on the rotation frequency; in particular from [9] we have

$$\begin{cases} \sigma_r = \dfrac{3+\kappa}{8}\rho {\omega_r}^2 {r_e}^2 \left(1 + \dfrac{{r_i}^2}{{r_e}^2} - \dfrac{{r_i}^2}{r^2} - \dfrac{r^2}{{r_e}^2}\right) \\ \sigma_t = \dfrac{3+\kappa}{8}\rho {\omega_r}^2 {r_e}^2 \left(1 + \dfrac{{r_i}^2}{{r_e}^2} + \dfrac{{r_i}^2}{r^2} - \dfrac{1+3\kappa}{3+\kappa}\dfrac{r^2}{{r_e}^2}\right) \end{cases}. \tag{14}$$

Considering the elongation along the radial and the tangential direction, the potential energy due to the tension is given by

$$V_{tens} = \int_S \left[\frac{\sigma_r r h}{2}\left(\frac{\partial w}{\partial r}\right)^2 + \frac{\sigma_t h}{2r}\left(\frac{\partial w}{\partial \vartheta}\right)^2\right] d\vartheta dr\,. \tag{15}$$

Following [10], the potential energy associated to the vibrations of the plate is given by

$$V_{elast} = \frac{1}{2}\left(\frac{Eh^3}{12(1-\kappa^2)}\right)$$
$$\int_S \left\{\left(\frac{\partial^2 w}{\partial r^2} + \frac{1}{r}\frac{\partial w}{\partial r} + \frac{1}{r^2}\frac{\partial^2 w}{\partial \vartheta^2}\right)^2 + \right.$$
$$\left. -2(1-\kappa)\frac{\partial^2 w}{\partial r^2}\left(\frac{1}{r}\frac{\partial w}{\partial r} + \frac{1}{r^2}\frac{\partial^2 w}{\partial \vartheta^2}\right) + \right.$$

$$+2(1-\kappa)\left[\frac{\partial}{\partial r}\left(\frac{1}{r}\frac{\partial w}{\partial \vartheta}\right)\right]^2\Bigg\} r d\vartheta dr \ . \qquad (16)$$

Considering the first mode and the corresponding eigenfunction 13, we can compare the two potential energies associated with centrifugal tensions and vibrations, by numerically calculating the two integrals 15 and 16. The ratio between these two energies can be considered as a meaningful parameter in estimating to what extent the rotation affects the natural vibration frequencies of the plate. Figure 10 shows the normalized frequency shift of the first mode $\Delta\omega_{1,0}/\omega_{1,0}$, given in table 6, versus the ratio between the two energies V_{tens}/V_{elast}. When the potential energy due to tension is negligible in comparison to the potential energy of vibrations, the effect of the inertia forces on the frequency is small, as in the case of true operating conditions of the grinder disk.

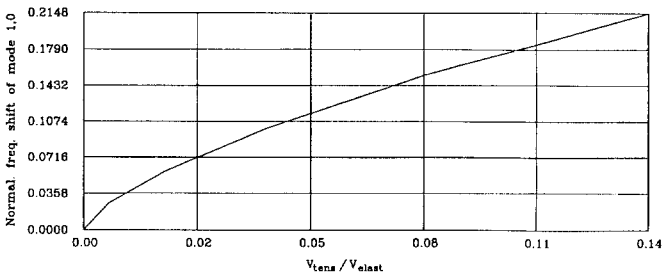

Figure 10: *Normalized frequency shift of the first mode.*

9 CONCLUSIONS

A comprehensive study on the vibrations of "normal" disks and the "Silentium" used in portable grinders, has been carried out. The main purpose of this article is to determine the elastic parameters and loss factor for these new "Silentium" disks. Having done this, it is possible to define the characteristics of the tested material, to predict the disks' natural frequencies and noise emission levels. The loss factor has been worked out from a series of acoustic measurements as described in section 3 for both classes of disks.

In the analysis different approaches have been followed: from the experimental investigation of the natural frequencies, the mode shapes and the loss factor have been calculated. By solving the equations governing the disk vibration, the experimental data have been theoretically validated. By comparing the experimental and the theoretical frequencies, the relevant constitutive parameters of the disks have been obtained. Through numerical analysis, the frequency shift due to the disk rotation has been taken into account.

From this composite analysis the following specific conclusions can be drawn. Due to its particular layered internal structure, the "Silentium" disk exhibits a significant damping of the high vibration modes. The experimental tests show that the ratio between the loss factors of the two disks can reach a value of up to three. This yields a peak amplitude reduction of 9.54 dB, thus confirming the efficiency of "Silentium" disk in limiting noise emission levels.

The theoretical frequencies correspond remarkably well to the experimental data. The analytical solution of the model together with the experimental data enables us to determine the elastic properties of the material. "Silentium" disks result as being less stiff and have a higher Poisson's ratio than "normal" disks.

10 ACKNOWLEDGMENTS

This work has been supported by MURST 1995 "Validazione dei meccanismi per l'automazione" U.O. Parma.

A APPENDIX

The matrix Z_n in equation 9 is given by:

$$Z_n = \begin{vmatrix} \zeta_{11} & \zeta_{12} & \zeta_{13} & \zeta_{14} \\ \zeta_{21} & \zeta_{22} & \zeta_{23} & \zeta_{24} \\ \zeta_{31} & \zeta_{32} & \zeta_{33} & \zeta_{34} \\ \zeta_{41} & \zeta_{42} & \zeta_{43} & \zeta_{44} \end{vmatrix} \qquad (17)$$

$$\begin{aligned} \zeta_{11} &= J_n & \zeta_{12} &= I_n \\ \zeta_{13} &= Y_n & \zeta_{14} &= K_n \\ \zeta_{21} &= \frac{n}{r_i}J_n - \gamma J_{n+1} & \zeta_{22} &= \frac{n}{r_i}I_n + \gamma J_{n+1} \\ \zeta_{23} &= \frac{n}{r_i}Y_n - \gamma Y_{n+1} & \zeta_{24} &= \frac{n}{r_i}K_n - \gamma K_{n+1} \end{aligned} \qquad (18)$$

with all Bessel functions calculated in γr_i ,

$$\zeta_{31} = \frac{n^2\eta}{r_e} J_n - (n^2\eta\gamma + \gamma^3)\left[\frac{n}{\gamma r_e} J_n - J_{n+1}\right]$$

$$\zeta_{32} = \frac{n^2\eta}{r_e} I_n - (n^2\eta\gamma - \gamma^3)\left[\frac{n}{\gamma r_e} I_n + I_{n+1}\right]$$

$$\zeta_{33} = \frac{n^2\eta}{r_e} Y_n - (n^2\eta\gamma + \gamma^3)\left[\frac{n}{\gamma r_e} Y_n - Y_{n+1}\right]$$

$$\zeta_{34} = \frac{n^2\eta}{r_e} K_n - (n^2\eta\gamma - \gamma^3)\left[\frac{n}{\gamma r_e} K_n - K_{n+1}\right]$$

$$\zeta_{41} = -\gamma r_e^3 \eta \left[\frac{n}{\gamma r_e} J_n - J_{n+1}\right] + r_e^2 \left(n^2\eta - \gamma^2\right) J_n$$

$$\zeta_{42} = -\gamma r_e^3 \eta \left[\frac{n}{\gamma r_e} I_n + I_{n+1}\right] + r_e^2 \left(n^2\eta + \gamma^2\right) I_n$$

$$\zeta_{43} = -\gamma r_e^3 \eta \left[\frac{n}{\gamma r_e} Y_n - Y_{n+1}\right] + r_e^2 \left(n^2\eta - \gamma^2\right) Y_n$$

$$\zeta_{44} = -\gamma r_e^3 \eta \left[\frac{n}{\gamma r_e} K_n - K_{n+1}\right] + r_e^2 \left(n^2\eta + \gamma^2\right) K_n \tag{19}$$

with all Bessel functions calculated in γr_e and $\eta = \dfrac{1-\kappa}{r_e^2}$.

The function given by $det(Z_n)$ only depends on the two products γr_i ,γr_e and on the two parameters n and κ . This can be verified multiplying by r_i the second row of Z_n and by ${r_e}^3$ the third row.

References

[1] H. Matsuhisa and S. Susumu 1986 *Noise Control Engineering Journal* **27**, 95-102. Noise from circular stone-sawing blades and theoretical analysis of their flexural vibrations.

[2] D. Rife and J. Vanderkooy 1989 *Journal of the Audio Engineering Society* **37**, 419-443. Transfer function measurements with maximum-length sequences.

[3] H. Alrutz and M. R. Schroeder 1983 *Proc. 11th Int. Congr. on Acoustics, Paris.* A fast Hadamard transform Method for evaluation of measurements using pseudo-random test signals.

[4] M. R. Schroeder 1965 *Journal of the Acoustic Society of America* **38**, 329-361 and **40**, 549-551. New method of measuring reverberation time.

[5] S. M. Voegel and D. W. Skinner 1965 *Journal of Applied Mechanics*, 926–921. Natural Frequencies of Transversely Vibrating Uniform Annular Plates.

[6] Lord Rayleigh 1987 *The Theory of Sound Vol.1.* New York: Dover Publications, second edition, 1945 re–issue.

[7] C. D'Angelo III, and C. D. Mote Jr 1993 *Journal of Sound and Vibration* **168**, 1–14. Natural Frequencies of a thin disk, clamped by thick collars with friction at the contacting surfaces, spinning at high rotation speed.

[8] P. J. Torvik *Damping Applications for Vibration Control* ASME AMD-38:85-112. The analysis and design of constrained layer damping treatments.

[9] Nuovo Colombo 1986 *Manuale dell'Ingegnere* **2**, F-159. Milano: Hoepli.

[10] S. Timoshenko,D. H. Young and W. Weaver Jr. 1974 *Vibration Problems in Engineering* . New York: Wiley.